Classification of noisy three-channel remote sensing images compressed by Versatile Video Coding*

Galina Proskura[1,*,†], Vladimir Lukin[1,†], Boban Bondžulić[2,†] and Dimitrije Bujaković[2,†]

[1] National Aerospace University, Department of Information-Communication Technologies, Vadyma Manka 17, Kharkiv 61070, Ukraine

[2] University of Defence in Belgrade, Military Academy, Veljka Lukića Kurjaka Street 33, Belgrade 11000, Serbia

Abstract

Spaceborne and airborne remote sensing (RS) systems produce data valuable for numerous applications. The amount of such data rapidly grows in general and for many particular systems in particular. It often becomes necessary to compress acquired images in a lossy manner providing a reasonable trade-off between compression ratio (CR) attained and image quality provided. Quality can be characterized from different viewpoints including classification accuracy observed for compressed data. A typical tendency is that this accuracy reduces if CR increases. However, there are specific situations when original images are noisy and, due to the specific effect of noise filtering by lossy compression, there can be the so-called optimal operation point (OOP) for which classification accuracy can be better than for original (uncompressed) images. OOP existence and properties depend on several factors including a coder used. In this paper, we employ the recently designed Versatile Video Coding (VVC) technique, which provides significant compression efficiency improvements over its predecessor HEVC. We demonstrate that, under certain conditions, OOP exists and show how it can be determined. Moreover, our studies indicate that lossy compression in OOP is able to produce improved classification accuracy simultaneously with rather large CR values. Experiments are carried out using two test three-channel RS images based on components of multispectral Sentinel data.

Keywords

remote sensing, neural classifier, noise, lossy compression, VVC, optimal operation point, classification accuracy [1]

1. Introduction

Images acquired by modern remote sensing (RS) systems are used in numerous applications [1-3]. Due to spatial resolution that steadily improves and more frequent observations of the Earth terrain, volume of acquired RS data increases [3-5]. This results in necessity to compress the obtained images for their transferring downlink, storage, and dissemination [5-7].

The image compression techniques belong to two large families – lossless and lossy [8]. For representatives of the former family, attained compression ratio (CR) values are usually too small. For lossy techniques, the main aspect is to provide a reasonable trade-off between quality and CR [5]. In remote sensing applications, quality can be treated in different ways. One option, as in conventional color images, is to consider standard criteria such as mean square error (MSE) or peak signal-to-noise ratio (PSNR) [5, 7] or visual quality metrics [9]. Meanwhile, since RS images are usually subject to some further analysis (segmentation, object detection, classification), other criteria and characteristics can be employed such as probability of correct classification (P_{cc}), confusion matrix, false alarm rate [10], etc.

As a rule, a larger CR leads to worse classification accuracy, although specific effects of better classification of compressed images (compared to uncompressed ones) are possible [11, 12]. Such

* CMIS-2026: The Ninth International Workshop on Computer Modeling and Intelligent Systems, May 05, 2026, Zaporizhzhia, Ukraine

[1*] Corresponding author.

[†] These authors contributed equally.

g.proskura@khai.edu (G. Proskura); v.lukin@khai.edu (V. Lukin); bondzulici@yahoo.com (B. Bondžulić); dimitrije.bujakovic@va.mod.gov.rs (D. Bujaković)

0000-0001-8960-0421 (G. Proskura); 0000-0002-1443-9685 (V. Lukin); 0000-0002-8850-9842 (B. Bondžulić); 0000-0001-7058-9293 (D. Bujaković)

effects often happen if compressed images are noisy [13] due to the fact that lossy compression of noisy images is characterized by a specific noise filtering effect. This effect was discovered about 30 years ago [14, 15]. Later it was studied for coders based on discrete cosine transform [16] according to conventional and visual quality metrics. Possible existence of the so-called optimal operation point (OOP) was shown [14-16] where OOP is a such value of a parameter that controls compression (PCC) for a given coder for which the compressed image is the closest to the corresponding true (noise-free) image according to a considered metric. Then, there are two reasons to compress noisy images in OOP (if it exists) or its close vicinity – to provide a relatively good quality of the compressed image and to produce CR considerably larger than for lossless and visually lossless compression. One more reason is that P_{cc} in OOP often occurs better than for original noisy data [13].

Performance characteristics of compression in OOP (if it exists) depend on many factors including image content, noise type and intensity, a used coder. When a new coder is introduced (such as, e.g., Better Portable Graphics (BPG) coder [17]), special studies are needed to develop methods for determining does OOP exist or no [16], what is PCC in OOP, etc.

Recently, Versatile Video Coding (VVC) has been proposed and studied in some papers [18-20], designed as a part of HEVC evolution [18]. It introduces numerous advanced coding tools such as a quadtree with nested multi-type tree partitioning, affine motion compensation, and adaptive loop filtering, which provide significant compression efficiency improvements compared to its predecessors. Although primarily intended for video, VVC can be effectively employed for other purposes, exploiting its advantages over existing techniques, such as the ability to provide larger CR for the same quality or better quality for the same CR [21, 22]. This was our main stimulus to consider VVC applicability to lossy compression of three-channel noisy RS images with special attention to analysis of classification accuracy. Another stimulus is that recently we have demonstrated the possible existence of OOP in lossy compression of noisy images by VVC and shown how OOP can be determined for the case of additive white Gaussian noise (AWGN) [23].

The main goal of this paper is to study classifier performance for uncompressed noisy and compressed three-channel noisy images of different complexity for VVC coding approach and neural network classifier. To the best of our knowledge, such a task has not been earlier considered and, thus, we are interested in producing practical recommendations and possible benefits of the proposed approaches.

2. Used images, noise model and quality criteria

In the experiments, we use two almost noise-free three-channel RS image fragments composed of visible bands of Sentinel-2 multispectral data (see 1). The images were acquired at the end of August 2019. Each fragment has a spatial size of 512×512 pixels with 8-bit representation per component.

The selected scenes differ in structural complexity. The first fragment (1a, SS1) corresponds to a rural area characterized by relatively large quasi-homogeneous regions. The second fragment (1b, SS2) represents an urban environment with a more complex spatial structure and a high density of fine details.

For both fragments, four thematic classes are considered: Urban, Water, Vegetation, and Bare Soil. Ground-truth labeling is available for both scenes, which enables quantitative evaluation of classification performance.

In practical RS systems, degradations may arise due to sensor limitations, acquisition conditions, and physical imaging principles. In this study, we adopt the AWGN model as a baseline statistical representation of noise.

(a) (b)

Figure 1: Image fragments used in simulations: (a) SS1, and (b) SS2.

For each channel $k \in \{1,2,3\}$, the observed pixel value at a spatial position (i,j) is modelled as:

$$I_{kij}^{noisy} = I_{kij}^{true} + n_{kij}, \tag{1}$$

where I_{kij}^{noisy} denotes the noisy ij-th pixel value, I_{kij}^{true} is the true ij-th pixel value, and n_{kij} is the value of AWGN having zero mean and variance σ^2.

The following assumptions are adopted: the noise is spatially uncorrelated, statistically independent across channels, and has identical variance in all three components. The variance is assumed to be known a priori or accurately estimated. Although real RS noise may exhibit signal dependency, after appropriate variance-stabilizing processing it can often be approximated by the AWGN model. Therefore, this model serves as a reasonable and analytically convenient starting point.

In the classification experiments, we analyze images corrupted by AWGN with variances $\sigma^2=50$ and $\sigma^2=100$. These values correspond to moderate and relatively strong noise levels for 8-bit data and allow studying the influence of noise intensity on classification accuracy under compression.

The noise level is characterized by the peak signal-to-noise ratio for the noisy image, defined as:

$$PSNR_k^n = 10\log_{10}\frac{255^2}{MSE_k^n} = 10\log_{10}\frac{255^2}{\sigma^2}\ [\text{dB}], \tag{2}$$

where MSE is the mean squared error between the true and noisy images, and 255 corresponds to the maximum possible pixel value in 8-bit representation.

Since the primary goal of the study is to evaluate the impact of compression on thematic mapping, classification-oriented metrics are used for performance assessment. The main evaluation measure is the F-measure, defined as the harmonic mean of precision and recall:

$$F = 2 \cdot \frac{precision \cdot recall}{precision + recall}, \tag{3}$$

For a given class, precision is defined as the proportion of correctly classified pixels among all pixels assigned to that class by the classifier. At the same time, recall is the proportion of correctly classified pixels among all reference pixels of that class.

We compute both the aggregated F-measure (F_{cc}), characterizing overall classification performance, and class-wise F-measures F_m, m=1, …, 4, that correspond to 1 – Urban, 2 – Water, 3 – Vegetation, and 4 – Bare Soil, respectively. This evaluation framework enables analysis of class

sensitivity to noise and compression distortions, as well as comparison of behavior between structurally simple and complex scenes.

3. Considered coder and basic rate-distortion curves

As the compression engine in this study, we employ VVC standard, specifically its VTM (VVC Test Model) reference software. VVC represents the state-of-the-art in video coding technology, offering significant compression efficiency improvements over its predecessors through advanced coding tools [18].

In VVC, the compression ratio is primarily controlled by the Quantization Parameter (QP), which determines the step size used for quantizing transform coefficients. Lower QP values result in finer quantization, leading to better reconstructed image quality at the expense of lower compression ratios (i.e., larger bitrates). Conversely, higher QP values produce coarser quantization, yielding higher compression ratios but reduced image quality. The QP range in VVC extends from 0 to 63, where 0 corresponds to nearly lossless compression and 63 to the highest compression ratio with the most significant quality degradation.

Since our work focuses on still image compression rather than video sequences, we operate VVC in intra-frame coding mode. Furthermore, given that our test images are three-channel color composites, we employ the 4:4:4 chroma format, which preserves full spatial resolution for all color components without subsampling. This ensures that the structural relationships between spectral bands are maintained during compression, which is particularly important for subsequent classification tasks where color information plays a crucial role.

In this paper, rate-distortion curves (RDCs) are presented as the dependence of objective quality on the QP parameter that controls VVC compression. 2 shows RDCs for three objective full-reference metrics: PSNR, SSIM (Structural Similarity Index) [24], and HaarPSI (Haar Wavelet-Based Perceptual Similarity Index) [25], computed for both compressed original noise-free images and compressed noisy images. PSNR is the most traditional metric. It is simple and widely used, but does not account for structural or perceptual image characteristics. SSIM evaluates image similarity through luminance, contrast, and structure comparisons. It is designed to better reflect human visual perception by focusing on structural information rather than pixel-wise errors. HaarPSI is a recent metric based on Haar wavelet decomposition. It analyzes images across multiple scales and incorporates weighting factors that correlate with human visual system sensitivity, aiming for high correlation with subjective quality assessments. For all three metrics, higher values indicate better quality. Here, these curves provide the foundation for understanding how compression parameter QP influence visual fidelity.

From 2a, which shows RDCs corresponding to compressed noise-free images, it can be observed that these curves are monotonically decreasing. Additionally, it can be noted that these curves depend on the source image content, which is particularly pronounced for the SSIM metric. These RDC shapes change significantly when compressing noisy images for the PSNR and SSIM metrics (2a and 2b). According to these two metrics, an OOP (maximum of objective quality) exists when compressing the noisy SS1 image, and according to PSNR, a weakly pronounced maximum also exists for the noisy SS2 image at variance 100. This confirms some earlier observations that the existence of OOP depends on the source image content, i.e., that the probability of OOP existence is higher for images that are less rich in details and contain smooth regions. Additionally, as the noise power increases, OOP positions shift to the right toward higher QP values. Thus, PSNR-based OOPs for image SS1 are 27 and 30, for noise variances 50 and 100, respectively. In contrast to these two metrics, HaarPSI RDCs for compressed noisy images are monotonically decreasing, so no OOPs are detected using this metric. Determining these objective scores requires access to the original images, so the use of these metrics is limited to laboratory tests or to their application in determining ground-truth OOPs.

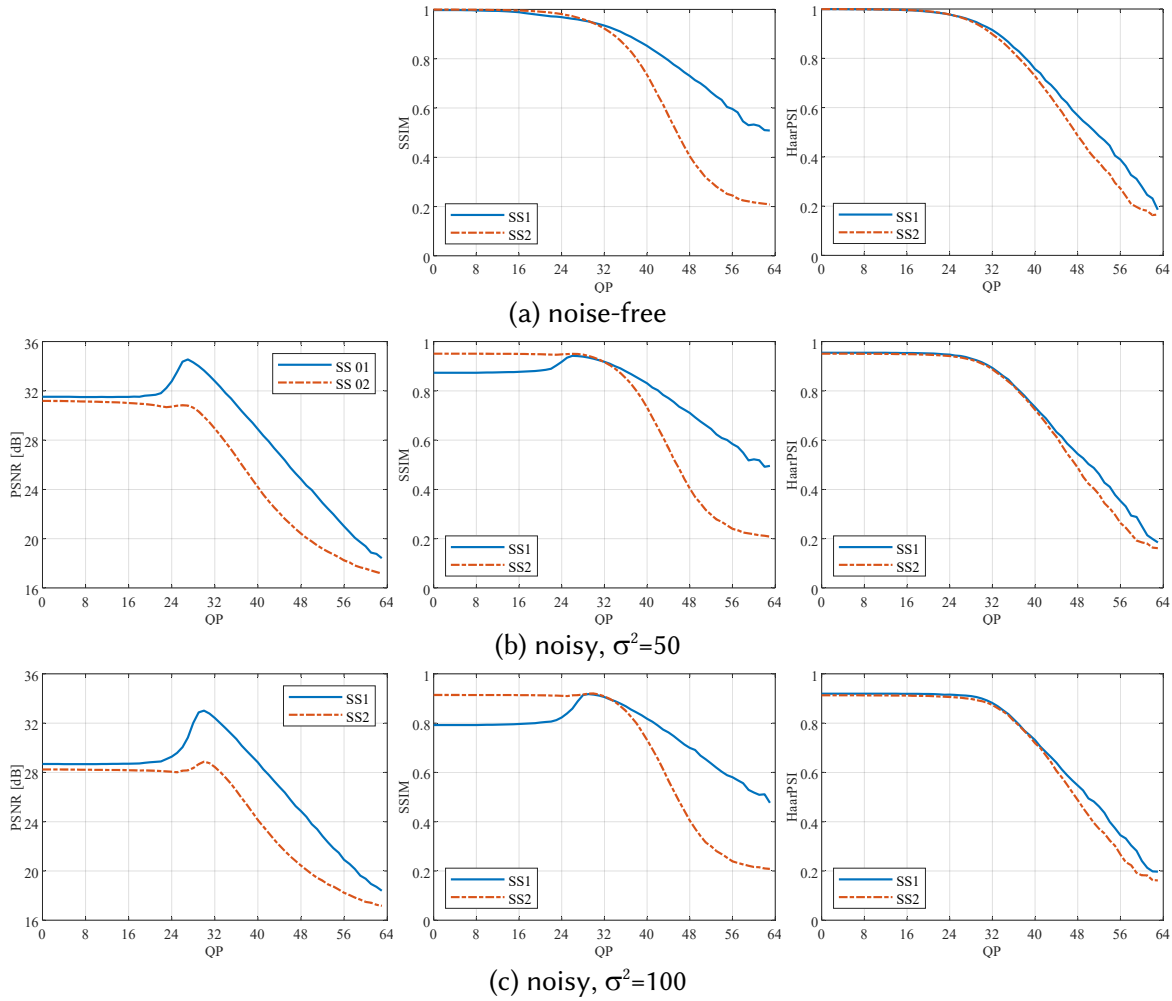

Figure 2: Full-reference metrics RDCs for: (a) noise-free, and (b) and (c) noisy compressed images.

In our previous research [26], based on the observed relationship between PSNR and QP at the OOP (QP_{OOP}), it was shown that a reliable prediction of QP_{OOP} can be obtained using the relation:

$$QP_{OOP} = 10.87 + 10\log_{10}\sigma^2. \quad (4)$$

The accuracy of this prediction depends on the noise variance estimation, for which reliable algorithms exist even for highly textured images [27]. For exact variance values (50 and 100), according to (4), the QP_{OOP} values are 28 and 31, respectively. This agrees with the PSNR- and SSIM-based OOPs. Even if an OOP does not exist, this prediction guarantees obtaining high-quality noisy compressed images (see RDCs in 2b and 2c; particularly note the HaarPSI RDCs), with quality almost identical to that achieved with compression at QP=0. Thus, we can also speak of a certain type of optimum here, which enables the maximum CR value while maintaining excellent visual quality.

An alternative to the full-reference are no-reference metrics, which do not require knowledge of the original image. In this paper, two variants of the well-known SISBLIM metric are selected, which is designed for quality assessment of singly and multiply distorted images [28]. These two variants ($SISBLIM_{sm}$ and $SISBLIM_{wm}$) employ distortion-specific quality measures intended for assessing blurring (using the same approach) and noise (using different approaches). 3 shows SISBLIM RDCs for compressed noise-free and noisy images, where lower metric values correspond to better quality.

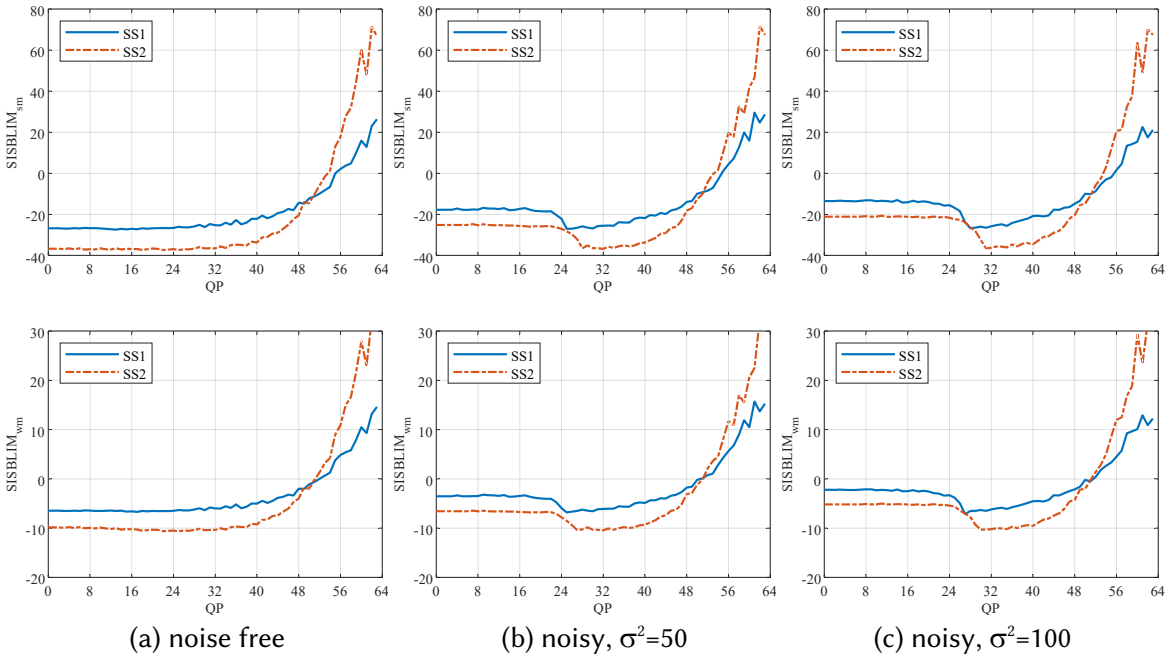

(a) noise free (b) noisy, σ^2=50 (c) noisy, σ^2=100

Figure 3: No-reference metrics RDCs for: (a) noise-free, and (b) and (c) noisy compressed images.

In this case as well, it can be concluded that the presence of noise in the image significantly affects the RDC profiles. Also, as the noise power increases, OOP positions shift to the right. Unlike full-reference metrics, the existence of OOP can be observed for both images and both noise levels. However, the OOP is not as pronounced since there is a range of QP values for which approximately the same quality values are obtained. Compared to OOPs detected with full-reference metrics, it can be said that no-reference-based OOPs lag by several QP values. Regardless of this difference, the goal of this paper is to examine classification accuracy in the vicinity of OOPs in the analysis that follows.

4. The studied classifier and its training

For three-channel RS images, various classification approaches can be applied [29, 30]. Based on previously obtained results [29], a feedforward neural network implemented as a sequential multilayer perceptron (MLP) is used in this study. The classifier is selected due to its relatively simple architecture, stable convergence properties, and sufficient representational capacity for low-dimensional spectral feature spaces.

Each pixel is represented by a three-dimensional feature vector corresponding to the visible spectral components. Before training, input data are normalized to the range [0, 1] by dividing pixel values by 255.

The network consists of five fully connected hidden layers containing 128, 64, 32, 16, and 8 neurons, respectively, followed by an output layer with Softmax activation. Hidden layers employ the ReLU activation function:

$$ReLU(x)=max(0,x), \tag{5}$$

which provides computational efficiency and favorable convergence behavior in deep networks.

The output layer produces posterior probabilities for five categories. Four neurons correspond to the thematic classes (Urban, Water, Vegetation, and Bare Soil), while the fifth neuron represents background/unlabeled pixels required for consistent mask-based processing. The final class label is assigned according to the maximum posterior probability criterion.

The network is trained in a supervised manner using sparse categorical cross-entropy as the loss function:

$$L = -\sum_{i} \log p_{y_i}, \tag{6}$$

where p_{y_i} denotes the predicted probability of the true class for pixel *i*.

Optimization is performed using the RMSProp algorithm, which is a modernized error backpropagation algorithm.

The network is trained for 70 epochs. Training loss and sparse categorical accuracy are monitored across epochs to ensure stable convergence. The network is trained using a batch size of 515 and default RMSProp parameters, without applying additional regularization techniques such as dropout or batch normalization.

For each 512×512 image fragment, spatial masks are constructed to divide pixels into training and test subsets. The masks used for the structurally simple and structurally complex images are shown in 4 and 5, respectively. The spatial masks are fixed across all experiments to ensure consistent evaluation conditions.

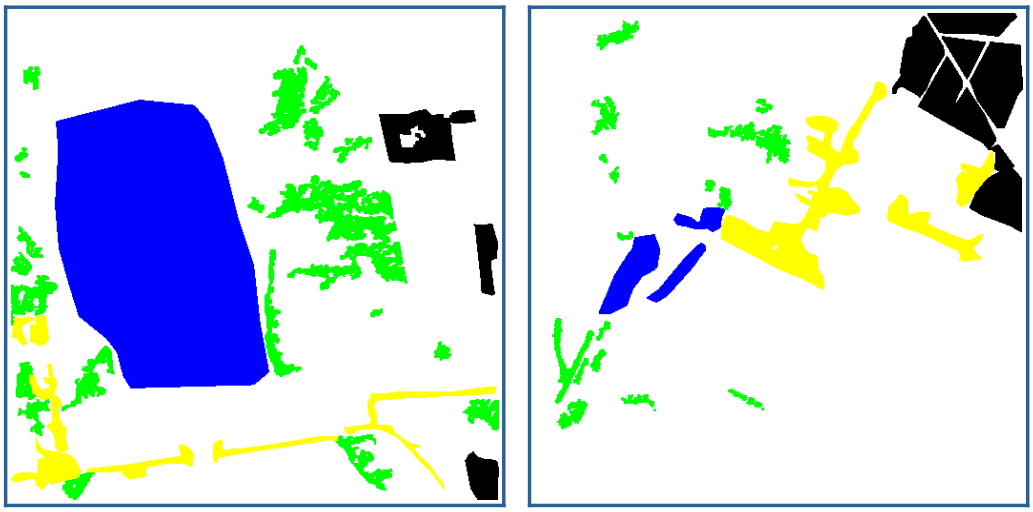

(a) (b)

Figure 4: Fragments employed for the classifier training for the test images:(a) SS1, and (b) SS2.

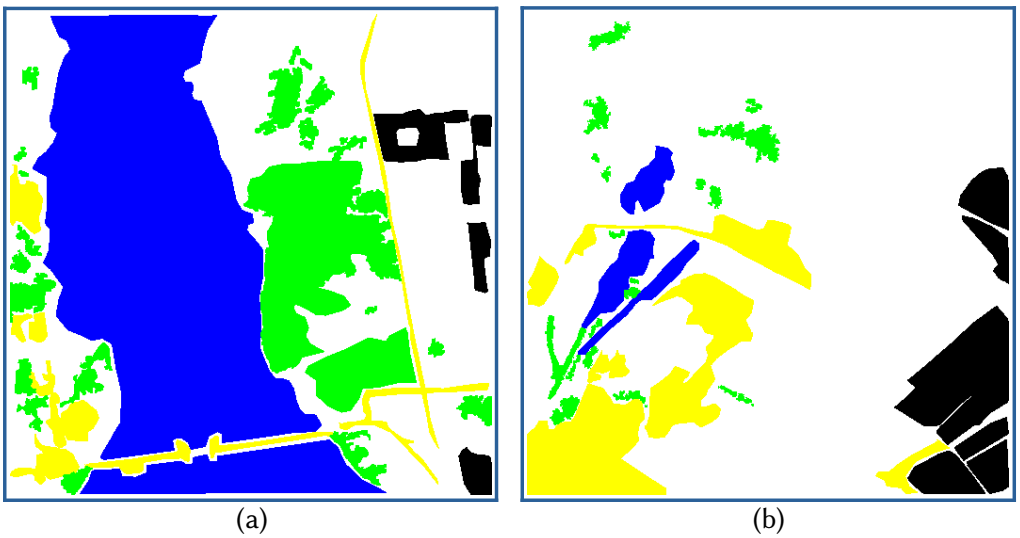

(a) (b)

Figure 5: Fragments employed for the classifier verification for the test images:(a) SS1, and (b) SS2.

Training and test regions are spatially separated in order to reduce statistical dependence between samples and to provide an unbiased estimation of classification performance. The corresponding training and verification sample sizes for SS1 and SS2 images are summarized in Table 1.

Table 1
The training and verification sample sizes for the test images

Class	SS1		SS2	
	Training samples, pixels	Verification samples, pixels	Training samples, pixels	Verification samples, pixels
Urban	7441	12154	11469	28040
Water	52310	96852	4201	7117
Vegetation	19936	38258	5993	6032
Bare Soil	6296	7898	15081	19125

5. Analysis of the obtained results

Recall that our classifier has been trained on noise-free images and then applied to noisy or noisy compressed images. This allows studying how noise and distortions due to lossy compression with different QP (and CR) influence classification accuracy in general and for particular classes. Thus, 2 presents class-wise and overall classification performance for noise-free, noisy, and noisy compressed images, together with the corresponding CR values of the noisy compressed images. Performance is presented for both noise variances and for several QP values. For convenience, we mark cases in the leftmost column. Analysis of data in 2 shows the following:

1. Noise presence leads to reduction of F_{cc} as well as F for all particular classes (consider Cases 1 and 8); the more intensive AWGN results in less F_{cc} and F for all particular classes (compare data for Cases 1 and 8); noise influence appears in multiple point-like misclassifications (compare data in 6a and 6b);
2. Lossy compression using $QP \leq QP_{OOP}-5$ does not make the classification results worse but, simultaneously, it does not lead to significant improvement of classification metrics (compare the Cases 1 and 2; compare the Cases 8 and 10);
3. For OOP or its close neighborhood (Case 3 for AWGN variance 50 and Case 11 for AWGN variance 100), the classification accuracy is considerably better than for the classifier applied to noisy images; it is comparable to classification data for the noise-free image (Case 0); see the classification map in 6c;
4. Meanwhile, even slightly better results have been obtained for $QP \approx QP_{OOP}+10$ (Cases 4-6 for AWGN variance 50 and Cases 12 and 13 for AWGN variance 100);
5. However, for QP>50, classification accuracy decreases and the obtained maps are characterized by artifacts (see the classification map in 6d);
6. Even for $QP \approx QP_{OOP}$ (Cases 3 and 11) the attained CR are large enough; furthermore, larger CR values can be provided if one sets QP slightly larger than QP_{OOP} without loss in classification accuracy.

Table 2
Classification accuracy for the test image SS1 particular classes, and general

Case	Noise variance	Image used for classification	F_1	F_2	F_3	F_4	Total F_{cc}	CR
0	-	noise-free	0.83	0.99	0.93	0.79	0.95	-
1	50	noisy	0.79	0.94	0.81	0.70	0.88	-
2	50	noisy, QP=22	0.79	0.95	0.84	0.70	0.89	5.37
3	50	noisy, QP=27	0.84	0.99	0.93	0.80	0.95	29.66
4	50	noisy, QP=32	0.83	0.99	0.92	0.83	0.95	69.74
5	50	noisy, QP=37	0.88	0.99	0.95	0.87	0.97	144.43
6	50	noisy, QP=42	0.81	0.99	0.95	0.83	0.96	288.28
7	50	noisy, QP=57	0.75	0.93	0.81	0.77	0.87	2488.7
8	100	noisy	0.77	0.88	0.71	0.59	0.81	-
9	100	noisy, QP=22	0.77	0.90	0.74	0.61	0.83	4.49
10	100	noisy, QP=27	0.77	0.96	0.87	0.70	0,91	13,19
11	100	noisy, QP=32	0.86	0.99	0.94	0.83	0.96	66.37
12	100	noisy, QP=37	0.86	0.99	0.95	0.84	0.96	143.56
13	100	noisy, QP=42	0.88	0.99	0.96	0.89	0.97	288.81
14	100	noisy, QP=52	0.78	0.98	0.92	0.71	0.94	1219.3
15	100	noisy, QP=57	0.70	0.85	0.70	0.61	0,78	2553,4

Let us now analyze the data in 3. The conclusions drawn are the following:

1. Noise results in reduction of F_{cc} as well as F for all particular classes (see data for Cases 1 and 9); the more intensive AWGN leads to smaller F_{cc} and F for all particular classes (compare data for Cases 1 and 9); the presence of noise in this case also leads to misclassifications (compare data in 7a and 7b);
2. Compression using $QP \le QP_{OOP}-5$ does not make the classification slightly better (compare the Cases 1 and 2 as well as the Cases 9 and 11);
3. For $QP_{OOP} \le QP \le QP_{OOP}+10$ the best classification results are obtained (Cases 3-6, Cases 12-15); accuracy is considerably better than for the classifier applied to noisy images (Case 1) and comparable to classification results for the noise-free image (Case 0); see the classification map in 7c;
4. For QP>45, classification accuracy decreases and the classification maps are characterized by artifacts (see 7d);
5. For $QP \approx QP_{OOP}$ (Cases 4 and 12) the attained CR are quite large although smaller than for SS1 image; larger CRs can be provided if QP is set slightly larger than QP_{OOP} practically without reduction of classification accuracy.

Table 3
Classification accuracy for the test image SS2 particular classes, and general

Case	Noise variance	Image used for classification	F_1	F_2	F_3	F_4	Total F_{cc}	CR
0	-	noise-free	0.93	0.78	0.68	0.91	0.87	-
1	50	noisy	0.83	0.48	0.49	0.72	0.71	-
2	50	noisy, QP=22	0.84	0.48	0.50	0.75	0.73	3.81
3	50	noisy, QP=27	0.91	0.70	0.61	0.90	0.85	7.59
4	50	noisy, QP=28	0.93	0.72	0.67	0.92	0.87	9.50
5	50	noisy, QP=32	0.94	0.70	0.72	0.95	0.89	17.93
6	50	noisy, QP=37	0.94	0.70	0.73	0.96	0.90	38.04
7	50	noisy, QP=42	0.91	0.62	0.60	0.91	0.85	98.99
8	50	noisy, QP=47	0.88	0.53	0.44	0.89	0.81	296.88
9	100	noisy	0.78	0.31	0.43	0.54	0.63	-
10	100	noisy, QP=22	0.80	0.37	0.44	0.60	0.66	3.38
11	100	noisy, QP=27	0.82	0.52	0.45	0.63	0.68	5.15
12	100	noisy, QP=31	0.93	0.68	0.65	0.92	0.87	14.05
13	100	noisy, QP=32	0.94	0.69	0.70	0.93	0.88	16.63
14	100	noisy, QP=37	0.94	0.69	0.68	0.95	0.88	37.00
15	100	noisy, QP=42	0.93	0.66	0.60	0.95	0.88	96.49
16	100	noisy, QP=47	0.91	0.68	0.46	0.94	0.85	292.14
17	100	noisy, QP=57	0.85	0.36	0.35	0.84	0,75	2721,2

Finally, our practical recommendations for applying VVC compression to noisy three-channel remote sensing images are the following: calculate QP_{OOP} based on objective quality metrics or depending on the noise variance; then use QP values larger than the determined QP_{OOP} (up to $QP_{OOP}+10$) to achieve good classification accuracy and rather large compression ratios; avoid using $QP \geq 50$ to prevent artifacts.

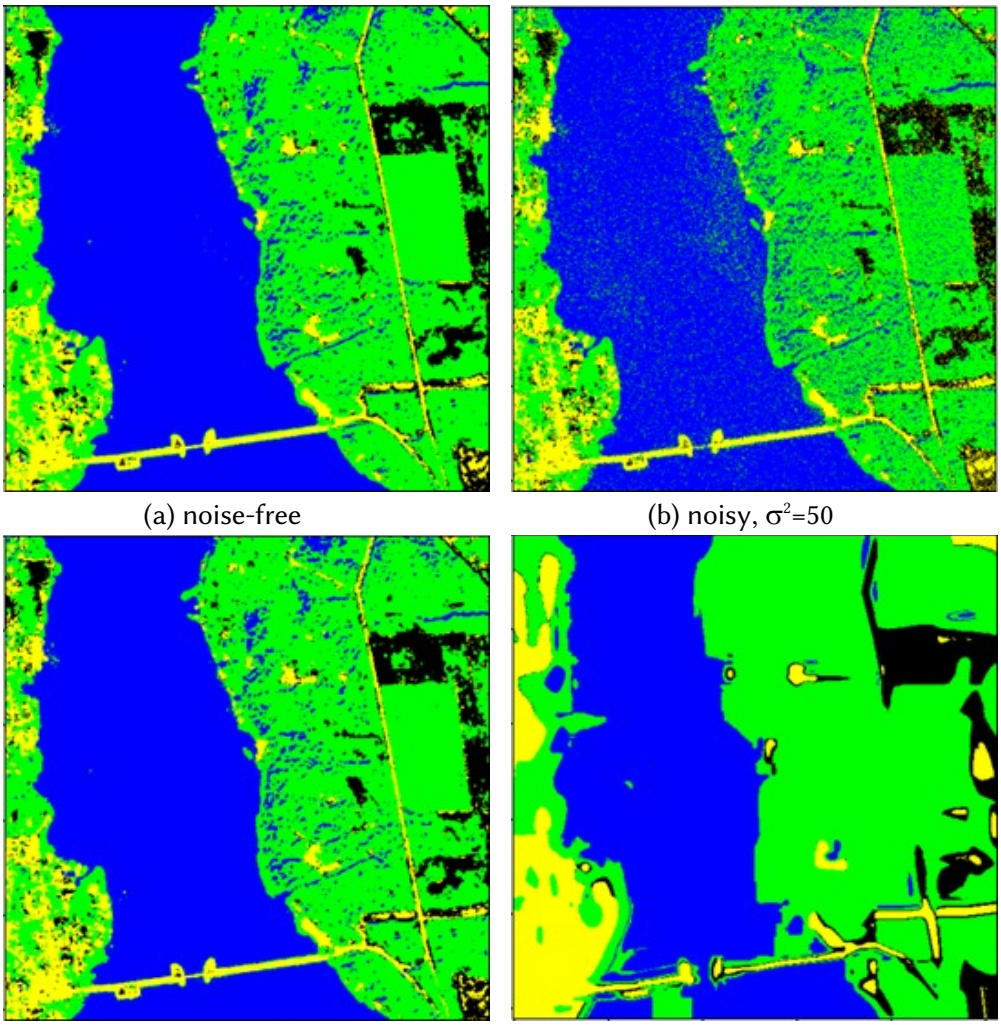

(a) noise-free (b) noisy, σ^2=50

(c) noisy, σ^2=50, QP=27 (d) noisy, σ^2=50, QP=57

Figure 6: SS1 image classification maps for: (a) Case 0, (b) Case 1, (c) Case 3, and (d) Case 7.

6. Conclusions

In this paper, the possibility of applying the VVC standard to noisy three-channel remote sensing images has been systematically investigated. The study was motivated by the need to achieve efficient compression of increasingly large volumes of remote sensing data while preserving or even improving the usability of such data for subsequent classification tasks.

It is shown that an optimal operation point (OOP) can exist according to different full-reference (PSNR, and SSIM) and no-reference ($SISBLIM_{sm}$ and $SISBLIM_{wm}$) metrics, approximately for the same QP values, where QP_{OOP} mainly depends on the noise variance. The likelihood of OOP existence is higher for larger noise variances and for images with simpler spatial structure, such as those containing large homogeneous regions. For images with complex structure (e.g., urban areas), the OOP is less pronounced but still observable under certain noise conditions. However, even if OOP does not exist for a given image, its lossy compression using QP_{OOP} calculated according to the proposed formula does not lead to a significant reduction of image quality.

Furthermore, lossy compression of noisy images in the vicinity of the OOP leads to improved classification accuracy, both in terms of aggregate criteria (F-measure) and per-class probabilities of correct classification. This improvement is observed not only at QP_{OOP} itself, but also, within certain limits, for QP values larger than QP_{OOP}, which allows for higher compression ratios while preserving or even enhancing classification performance. Such benefits are attainable even for images with complex structure, although the achievable compression ratios may be somewhat

lower compared to simpler images. However, for QP≥50, compression artifacts begin to appear, affecting both visual quality and classification accuracy. This indicates that there is an upper bound on QP beyond which compression becomes detrimental regardless of noise level.

The results also demonstrate that VVC, operating in intra-mode with 4:4:4 chroma format, is well-suited for remote sensing image compression, offering not only state-of-the-art compression efficiency but also the potential to exploit noise filtering effects for improved classification accuracy.

In future work, we plan to extend the analysis to a larger set of test images covering diverse land cover types and acquisition conditions. We also intend to investigate other types of classifiers, including deep learning-based approaches, and to explore the possibility of adapting compression parameters based on image content and noise characteristics. Additionally, the influence of more complex noise models (e.g., signal-dependent noise) on OOP existence and classification accuracy will be addressed.

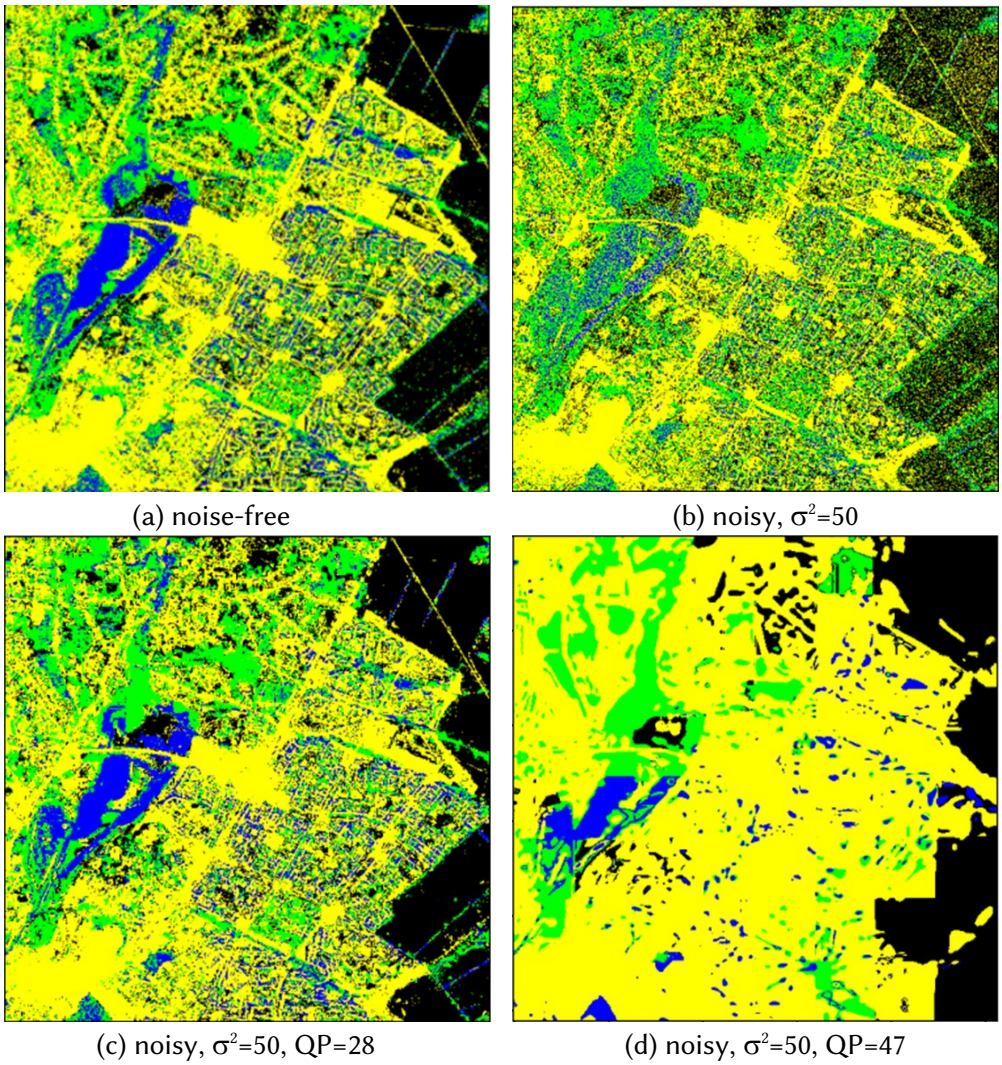

Figure 7: SS2 image classification maps for: (a) Case 0, (b) Case 1, (c) Case 4, and (d) Case 8.

Declaration on Generative AI

During the preparation of this work, the authors used DeepSeek in order to: Grammar and spelling check. After using this tool, the authors reviewed and edited the content as needed and took full responsibility for the publication's content.

References

[1] B. Aiazzi, L. Alparone, S. Baronti, C. Lastri, M. Selva, Spectral distortion in lossy compression of hyperspectral data, Journal of Electrical Computer Engineering, art. no. 850637 (2012) 1–8. doi:10.1155/2012/850637.

[2] E. Dritsas, M. Trigka, Remote sensing and geospatial analysis in the big data era: A survey, Remote Sensing 17.3, art. no. 550 (2025) 1–30. doi:10.3390/rs17030550.

[3] S. Khorram, C. F. van der Wiele, F. H. Koch, S. A. C. Nelson, M. D. Potts, Future trends in remote sensing, in: Principles of Applied Remote Sensing, Springer, Cham, 2016, pp. 277–285. doi:10.1007/978-3-319-22560-9_9.

[4] I. Vasilyeva, V. Lukin, V. Kharchenko, A. Nereta, Combined processing of satellite and UAV data to increase the classification reliability, Proceedings of the 4th International Workshop on Intelligent Information Technologies & Systems of Information Security, 2023, pp. 539–552. URL: https://ceur-ws.org/Vol-3373/paper37.pdf.

[5] E. Christophe, Hyperspectral data compression tradeoff, in: S. Prasad, L. Bruce, J. Chanussot (Eds.), Optical Remote Sensing, Augmented Vision and Reality, vol. 3, Springer, Berlin, Heidelberg, 2011, pp. 9–29. doi:10.1007/978-3-642-14212-3_2.

[6] S. Doss, S. Pal, D. Akila, S. Jeyalaksshmi, T. N. Jabeen, G. Suseendran, Satellite image remote sensing for identifying aircraft using SPIHT and NSCT, Journal of Critical Reviews 7.5 (2020) 631–634.

[7] D. Tao, S. Di, X. Liang, Z. Chen, F. Cappello, Fixed-PSNR lossy compression for scientific data, Proceedings of the IEEE International Conference on Cluster Computing (CLUSTER), Belfast, UK, 2018, pp. 314–318. doi:10.1109/CLUSTER.2018.00048.

[8] A. J. Hussain, A. Al-Fayadh, N. Radi, Image compression techniques: A survey in lossless and lossy algorithms, Neurocomputing 300 (2018) 44–69. doi:10.1016/j.neucom.2018.02.094.

[9] G. Zhai, X. Min, Perceptual image quality assessment: A survey, Science China Information Sciences 63.11, art. no. 211301 (2020) 1–52. doi:10.1007/s11432-019-2757-1.

[10] J. L. García-Balboa, M. V. Alba-Fernández, F. J. Ariza-López, J. Rodríguez-Avi, Analysis of thematic similarity using confusion matrices, ISPRS International Journal of Geo-Information 7.6, art. no. 233 (2018) 1–10. doi:10.3390/ijgi7060233.

[11] A. Zabala, X. Pons, Effects of lossy compression on remote sensing image classification of forest areas, International Journal of Applied Earth Observation and Geoinformation 13.1 (2011) 43–51. doi:10.1016/j.jag.2010.06.005.

[12] N. Ozah, A. Kolokolova, Compression improves image classification accuracy, in: M. J. Meurs, F. Rudzicz (Eds.), Advances in Artificial Intelligence, Canadian AI 2019, Lecture Notes in Computer Science, vol. 11489, Springer, Cham, 2019, pp. 525–530. doi:10.1007/978-3-030-18305-9_55.

[13] G. Proskura, V. Naumenko, V. Lukin, Classification of BPG-based lossy compressed noisy images, Ukrainian Journal of Remote Sensing 11.3 (2024) 13–25. doi:10.36023/ujrs.2024.11.3.266.

[14] S. G. Chang, B. Yu, M. Vetterli, Image denoising via lossy compression and wavelet thresholding, Proceedings of the International Conference on Image Processing, Santa Barbara, CA, USA, 1997, vol. 1, pp. 604-607. doi:10.1109/ICIP.1997.647985.

[15] O. K. Al-Shaykh, R. M. Mersereau, Lossy compression of noisy images, IEEE Transactions on Image Processing 7.12 (1998) 1641-1652. doi:10.1109/83.730376.

[16] V. Lukin, B. Kovalenko, S. Kryvenko, N. Ponomarenko, K. Egiazarian, J. Astola. Compression of noisy images taking into account visual quality: A comprehensive study, in: J. Purenović (Ed.), Research Developments in Science and Technology, vol. 8, Book Publisher International, 2022, pp. 89–109. doi:10.9734/bpi/rdst/v8/2722B.

[17] U. Albalawi, S. P. Mohanty, E. Kougianos, Energy-efficient design of the secure Better Portable Graphics compression architecture for trusted image communication in the IoT, Proceedings

of the IEEE Computer Society Annual Symposium on VLSI (ISVLSI), Pittsburgh, PA, USA, 2016, pp. 302–307. doi:10.1109/ISVLSI.2016.21.
[18] B. Bross et al., Overview of the Versatile Video Coding (VVC) standard and its applications, IEEE Transactions on Circuits and Systems for Video Technology 31.10 (2021) 3736–3764. doi:10.1109/TCSVT.2021.3101953.
[19] D.-H. Kim, J. Young Jeong, G. Lee, J.-G. Kim, Compression method of NeRF model using NNC and VVC, Proc. SPIE 13164, International Workshop on Advanced Imaging Technology (IWAIT), 131642V (2024) 1–6. doi:10.1117/12.3019533.
[20] S. Bouaafia, Optimization and acceleration of HEVC and VVC video compression standards using artificial intelligence on parallel processing platforms, Ph.D. thesis, University of Monastir, Monastir, Tunisia, 2021. URL: https://theses.hal.science/tel-04098015.
[21] M. Uhrina, L. Sevcik, J. Bienik, L. Smatanova, Performance comparison of VVC, AV1, HEVC, and AVC for high resolutions, Electronics 13.5, art. no. 953 (2024) 1–21. doi:10.3390/electronics13050953.
[22] D. Petreski, T. Kartalov, Next generation video compression standards – Performance overview, Proceedings of the 30th International Conference on Systems, Signals and Image Processing (IWSSIP), Ohrid, North Macedonia, June 27–29, 2023, pp. 1-5. doi:10.1109/IWSSIP58668.2023.10180261.
[23] B. Bondžulić, V. Lukin, D. Bujaković, B. Kovalenko, VVC compression of noisy three-channel images with no-reference metrics analysis, 15th International Conference on Dependable Systems, Services and Technologies (DESSERT'2025), Athens, Greece, December 19–21, 2025. To appear.
[24] Z. Wang, A. C. Bovik, H. R. Sheikh, E. P. Simoncelli, Image quality assessment: From error visibility to structural similarity, IEEE Transactions on Image Processing 13.4 (2004) 600–612. doi:10.1109/TIP.2003.819861.
[25] R. Reisenhofer, S. Bosse, G. Kutyniok, T. Wiegand, A Haar wavelet-based perceptual similarity index for image quality assessment, Signal Processing: Image Communication 61 (2018) 33–43. doi: 10.1016/j.image.2017.11.001.
[26] M. Z. Laidouni, T. Adli, B. Bondžulić, V. Lukin, B. Kovalenko, S. Kryvenko, Optimal operation point analysis in VVC-based compression of noisy remote sensing images, Proceedings of the 18th IEEE International Conference on Advanced Trends in Radioelectronics, Telecommunications and Computer Engineering (TCSET), Lviv, Ukraine, February 17–21, 2026, pp. 1–6. doi:10.1109/TCSET65181.2026.11461063.
[27] M. Ponomarenko, N. Gapon, V. Voronin, K. Egiazarian, Blind estimation of white Gaussian noise variance in highly textured images, Electronic Imaging 30.13 (2018) 382-1-382–5. doi:10.2352/ISSN.2470-1173.2018.13.IPAS-382.
[28] K. Gu, G. Zhai, X. Yang, W. Zhang, Hybrid no-reference quality metric for singly and multiply distorted images, IEEE Transactions on Broadcasting 60.3 (2014) 555–567. doi:10.1109/TBC.2014.2344471.
[29] G. Proskura, I. Vasilyeva, F. Li, V. Lukin, Classification of compressed multichannel images and its improvement, Proceedings of the 30th International Conference Radioelektronika (RADIOELEKTRONIKA), Bratislava, Slovakia, April 15–16, 2020, pp. 1–6. doi:10.1109/RADIOELEKTRONIKA49387.2020.9092371.
[30] V. Makarichev, I. Vasilyeva, V. Lukin, B. Vozel, A. Shelestov, N. Kussul, Discrete atomic transform-based lossy compression of three-channel remote sensing images with quality control, Remote Sensing 14.1, art. no. 125 (2022) 1–35. doi:10.3390/rs14010125.